Theoretical Chemistry Accounts (2019) 138:120
https://doi.org/10.1007/s00214-019-2507-1

REGULAR ARTICLE

Examination of the performance of semiempirical methods in QM/MM studies of the S_N2-like reaction of an adenylyl group transfer catalysed by ANT4′

Sergio Martí[1] · Vicent Moliner[1] · Katarzyna Świderek[1]

Received: 11 April 2019 / Accepted: 19 September 2019 / Published online: 9 October 2019

Abstract

Quantum mechanical (QM) semiempirical methods (SMs), combined with molecular mechanics (MM) force fields, are extensively used in theoretical studies of enzymatic reactions. Despite being several orders of magnitude faster than ab initio methods, their correctness is essential to be used in calculations requiring statistical simulations. Herein, a wide range of SMs are examined, from those based on s and p orbitals, *sp*-SMs (MNDO, AM1, PM3 and RM1), to those including d orbitals, *spd*-SMs, either based on approximations to the Hartree–Fock theory (MNDO/d, PM6 and AM1/d-PhoT) or derived from density functional theory (DFTB3). These QM Hamiltonians are used within a multiscale QM/MM additive scheme, to clarify their usefulness in mechanistic studies of phosphoryl-transfer reactions. The S_N2-like reaction of the adenylyl group transfer catalysed by 4′-O-Nucleotidyltransferase (ANT4′) was selected as a benchmark. Geometrical characteristics of stationary structures, the shape of potential energy surfaces together with the barrier heights and kinetic isotope effects (KIEs), obtained with the different SMs/MM methods were compared with results obtained at higher M06-2X/MM level of theory. Critical limitations of the *sp*-SMs in the present mechanistic study were detected. The *spd*-SMs describe the reaction as a concerted process, same as the reference method M06-2X, but none of them is free of limitations. PM6 reproduces the biased trend of previous sp-SMs stabilizing structures of phosphorous atoms with certain pentavalent character, while AM1/d-PhoT and DFTB3 describe TSs more dissociative than M06-2X, which determines the lower quality of the computed primary and secondary $^{16}O/^{18}O$ KIEs. Efforts to improve the SMs can be guided by the exposure of their limitations, which were supported by the results of a second studied phosphoryl-transfer reactions; the hydrolysis of phosphodiester bond at the 3′-end of the viral DNA (vDNA). Thus, for instance, further increases in SMs accuracy can be achieved by improving the training and survey reference data sets, a more complete set of parameters for describing intermolecular interactions or further developments of *spd*-SMs.

Keywords Adenylyl transfer · Semiempirical methods · M06-2X · QM/MM · Phosphate chemistry

1 Introduction

The molecules involved in chemical reactions catalysed by enzymes are surrounded by a fluctuating environment of protein and solvent [1]. Thus, accurate theoretical calculations of rate constants, binding processes and isotope effects, including the possible impact of quantum tunnelling, dynamic or electrostatic effects in this type of biological models requires introduction of the environmental diversity [2–5]. Methods based on density functional theory (DFT) are powerful and efficient for calculating potential energy surfaces (PES) for chemical reaction. Nevertheless, in case of processes occurring in active sites of enzymes, they are often prohibitively expensive, especially to perform

Published as part of the special collection of articles derived from the 11th Congress on Electronic Structure: Principles and Applications (ESPA-2018).

Electronic supplementary material The online version of this article (https://doi.org/10.1007/s00214-019-2507-1) contains supplementary material, which is available to authorized users.

✉ Vicent Moliner
moliner@uji.es

✉ Katarzyna Świderek
swiderek@uji.es

[1] Departament de Química Física i Analítica, Universitat Jaume I, 12071 Castellón, Spain

statistical simulations [6]. The most promising alternative is the use of hybrid quantum mechanics/molecular mechanics (QM/MM) potentials. Nowadays, the two most common schemes to get the energy of a molecular system in QM/MM simulations are those based on molecular orbital (MO) treatments in which the wave function of the QM subsystem is obtained under the effect of the environment that is treated by means of a classical molecular mechanics (MM) force fields [7], and methods based in valence-bond descriptions, known as empirical valence bond (EVB) methods, where the QM subsystem is described by means of two or more valence states, each one described with its MM force field that allows for the interaction with the surroundings and mixed through an off-diagonal Hamiltonian parameterized term [8]. In any case, when computing rate constants for chemical reactions taking place in the active site of an enzyme, an extensive sampling is required to get activation and reaction free energies, which are the magnitudes that can be directly compared with the experimentally determined rate and equilibrium constants. These simulations are usually performed by means of molecular dynamics (MD) or Monte Carlo (MC) techniques. QM/MM MD simulations are quite popular nowadays, but the computational cost of the simulations limits the timescale of the samplings. Consequently, these kind of simulations typically employ semiempirical methods (SMs) to describe the QM subset of atoms. Thus, considering the value but also the intrinsic limitations associated to SMs, their benchmark and correctness are crucial.

Many examples have been studied in our laboratory where the chemistry of an enzymatic reaction is described in a sufficient way by SMs [9–13]. However, there are cases like, for instance, those involving the transfer of light particles that require improvement of the semiempirical Hamiltonian. Overcoming the SMs deficiency was partially achieved by modifying parameters of existing classical SMs. One of the strategies was the development of new parameters specially designed for studies of specific reactions, such as the specific reaction parameters for AM1 method (AM1-SRP) used in the studies of hydride transfer reaction catalysed by dihydrofolate reductase (DHFR) [14] and formate dehydrogenase (FDH) [15], or proton transfer occurring in the active site of alanine racemase (AR) [16]. A PM3-SRP method was used when the available SMs failed in prediction of frequency value corresponding to the stretching mode of the nitrile bond to study the vibrational Stark effect [17]. Unfortunately, the biggest disadvantage of SRP-SMs is the lack of universality. As previously shown, the results derived from different SRP-SMs methods can differ meaningfully [18].

Another important group of enzymatic reactions that has been demonstrated to be particularly challenging for the selection of a proper QM method in QM/MM simulations are those involving a phosphate atom. Despite extensive efforts from both experimental and theoretical studies, the precise mechanism of phosphate chemistry such as phosphate hydrolysis and phosphoryl transfer remains controversial [19–23]. This is a major problem to solve because phosphate chemistry plays a key role in many essential biological processes such as energy/signal transduction and synthesis of protein and nucleic acids. From a theoretical point of view, it is crucial to possess an effective computational QM method that can balance accuracy and sampling efficiency required in QM/MM MD simulations. There have been several such models developed in recent years for specific types of phosphate reactions [24–27], although their general applicability still remains to be fully explored. In view of these limitations, Marcos et al. tested the performance of SMs in describing phosphate transfer reactions with QM/MM methods, concluding that the best methods to describe penta-coordinated structures are PM6 and AM1/d-PhoT and for energetics AM1/d-PhoT [28]. Nevertheless, more recent studies where AM1/d-PhoT was chosen to describe the QM region have questioned its capability to get reliable geometries [29, 30].

Herein, we investigate the usefulness of different kinds of SMs in describing an O-P bond cleavage process. SMs based on the use of just *sp* basis sets, such as the Modified Neglect of Diatomic Overlap (MNDO) [31], Austin Model 1 (AM1) [32], parametric method number 3 (PM3) [33] or a Reparametrized AM1 (RM1) [34], are widely used in theoretical studies of molecular structure and reactivity, should not be used in the systems with transition metal compounds. The lack of *d* orbitals is believed to be responsible for the destabilization of hypervalent species of main-group elements [33]. Despite it is assumed that this problem was overcome by enhanced parametrization of PM3 method [24], the improved versions of standard *sp*-SMs still present serious limitations to be considered as universal.

Historically, the first semiempirical method improved by incorporating *d* orbitals, the *spd*-SMs group, was MNDO-d [35, 36]. However, the MNDO and MNDO-d models are known to be problematic in the description of noncovalent intermolecular interactions because of the extensive repulsion just outside bonding distances [24]. More recent semiempirical methods have tried to improve these interactions through different types of modifications. However, newer methods (AM1 and PMn families) rely on the "brute-force" core–core repulsion function proposed by Dewar for AM1 and modified by Stewart for PM3. It was shown that such repulsion functions lead to unphysical artefacts in the intermolecular interactions [37], which significantly limits the use of the methods in chemical reactivity, more particularly in those involving enzymatic processes. Some possible solutions were proposed for this issue that not only improves the potential energy surfaces but also the energetics of proton transfer (pKa) [37–40]. Improvement of these limitations

became the reason of development of PM6 [41], successfully used for modelling a large number of properties of proteins, including metalloproteins [42]. Note that the above-mentioned artefacts favour very short non-bonded H···H distances and are present not only in the original AM1 and PM3 methods but also in PM6 and others [43]. AM1/d [44] method and its version containing specific reaction parameters for phosphoryl-transfer reactions AM1/d-PhoT [24] was also developed for the study of these kind of phosphorous containing systems. Finally, semiempirical density functional tight binding (DFTB3 ob-3-1, DFTB3 from now on) [45–47] method, based on a Taylor expansion of the energy with respect to a reference density, was more recently developed and has been suggested as a promising tool [48].

The examination carried out in the present paper is based on the S_N2-like reaction mechanism of the adenylyl group transfer catalysed by 4′-O-Nucleotidyltransferase (ANT4′), enzyme involved in origin of the bacterial resistance [49, 50]. In this particular process, aminoglycoside antibiotic (Kanamycin A) is modified by ANT which promotes reaction between MgATP and antibiotic allowing to form O-adenylylated aminoglycoside and the magnesium chelate of inorganic pyrophosphate ($MgPP_i$), as presented in Scheme 1. This reaction belongs to the group of very important processes involved in worldwide problems of increasing bacterial resistance on drugs [51]. The mechanism of this reaction was previously studied [52] in details at DFT/MM level using M06-2X [53, 54] method with 6–31 + $G(d, p)$ basis set. As it was shown, adenylyl group is transferred from ATP-cofactor to KanA in a concerted manner where the nucleophilic attack of O4′ to Pα takes place together with the Pα-O3α bond cleavage, concomitant with the transfer of H4′ from O4′ to the oxygen of Glu145 (see Scheme 1). These results, together with the optimized and characterized stationary structures, potential energies and kinetic isotope effects (KIEs), served as a benchmark for the validation of the SMs methods selected in the present study. The present systematic study of the different possible choices of QM SMs can complement those previously carried out in our laboratory for the phosphoryl-transfer reaction between adenosine triphosphate (ATP) and dihydroxyacetone (Dha) in aqueous solution [55], or catalysed by DhaK from Escherichia coli [56], and the phosphoryl-transfer reaction from an inorganic polyphosphate to Dha catalysed by DhaK from C. freundii [22].

2 Computational methods

2.1 Setup of the system

A molecular model of aminoglycoside ANT4′ was built based on the structure available in the Protein Data Bank with code 1KNY [57]. The non-hydrolysable adenosine 5′-triphosphate (ATP) cofactor, AMPCPP, was modified to ATP. Missing hydrogen atoms were added taking into account the pK_a values of titratable aminoacids computed with PropKa program [58]. Subsequently, 40 Na^+ counterions were added and the complete system was solvated with a $10 \times 10 \times 10$ nm^3 box of water molecules. The detailed description of the each step of preparation of this system for theoretical studies can be found elsewhere [52].

2.2 QM/MM calculations

The potential energy of the QM/MM system was computed according to equation:

$$E_{\text{tot}} = E_{\text{QM}} + E_{\text{QM/MM}} + E_{\text{MM}} = \Psi \left| \hat{H}_0 \right| \Psi + \Psi \left| \hat{V} \right| \Psi + E_{\text{MM}}$$

where $\hat{H}_0$ is the in vacuum semiempirical Hamiltonian for the selected SMs, Ψ is the polarized wave function originated in the presence of a flexible distribution of point charges, representing the MM atoms, $\hat{V}$ describes the coupling (electrostatic and van der Waals) operator between the QM and MM subsystems and E_{MM} represents the force field energy. Herein, eight different semiempirical Hamiltonians

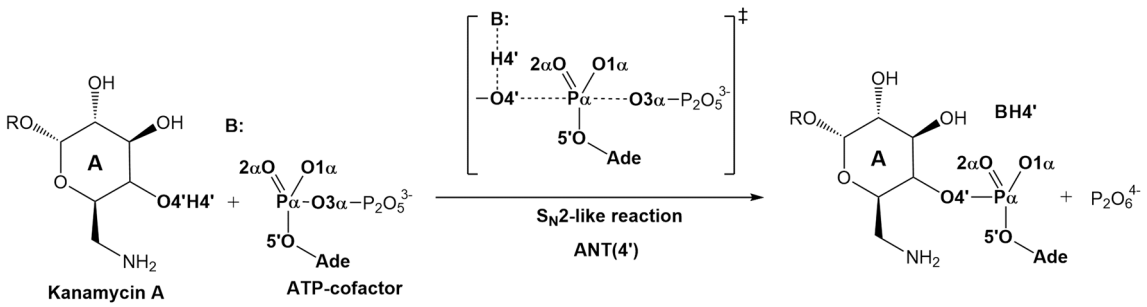

Scheme 1 S_N2-like reaction of the adenylyl group transfer from ATP-cofactor to Kanamycin A in the active site of ANT4′. The role of the base (B:) is played by Glu145 of ANT4′

were applied to describe the QM subset of atoms, as shown in Scheme 2. Four *sp* basis set SMs, such as MNDO, AM1, PM3 and RM1 were selected. In addition, three *spd*-SMs methods, MNDO/d, PM6 and AM1/d-PhoT were added into the benchmarking. Finally, recently developed DFTB method was also examined. The MM region in all calculation was described by AMBER [59] force field as implemented in the fDynamo [60, 61] library, and the TIP3P force field for the water molecules [62]. The standard MOPAC [63] sp-SMs (MNDO, AM1, PM3 and RM1) were used as implemented in the fDynamo library. In order to use spd-SMs as well as DFTB3 methods, the SQM as implemented in AmberTools16 [64] program was combined with fDynamo.

2.3 Potential energy surfaces (PESs)

In order to explore the reaction mechanisms, two-dimensional (2D) QM/MM PESs were computed with all tested methods. These PESs were obtained by restraining those key distances which mostly represent the reaction coordinate. In particular, the anti-symmetric combination of the distances describing the nucleophilic attack of O4′ to Pα and the Pα-O3α bond cleavage, together with the anti-symmetric combination of the distances describing the transfer of H4′ from O4′ to the oxygen of Glu145, were controlled by applying a force constant of 5000 kJ mol^{-1} $Å^{-1}$, with a size step 0.05 Å for proton transfer and 0.1 Å for bond formation and cleavage between heavy atoms.

2.4 Localization of the stationary structures

The initial structures for transition states (TS) search were extracted from the quadratic region of the explored PESs and were compared with the structures previously localized at M06-2X/MM level. Optimization of the TS structures with

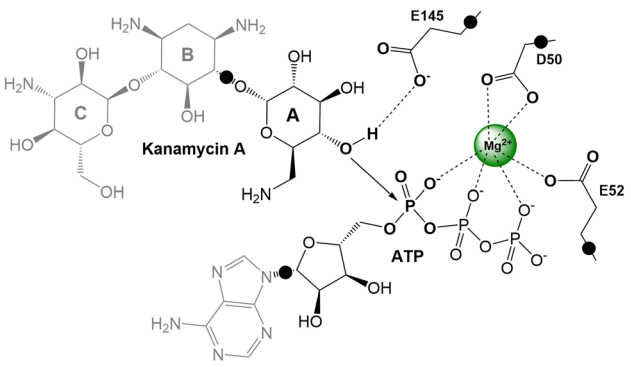

Scheme 2 Structure of the active site of ANT4′ representing the atoms of QM region. Atoms in grey of KanA and ATP, as well as the rest of protein and water molecules, were treated by MM force fields. Black dots indicate link atoms

different semiempirical Hamiltonians was achieved by combining macroiterations based on the L-BFGS-B minimization routine [65] with microiterations guided by the BAKER algorithm: [66, 67] the negative selected eigenvector of the Hessian matrix is maximized, while the rest are minimized. The modified BAKER algorithm with respect to the originally implemented in fDynamo was used, to be able to work in a micro/macroscheme [68, 69]. By following the direction specified by the transition vector in the localized TSs, the paths of the chemical reaction were traced by using intrinsic reaction coordinates (IRCs) [70] to the valleys of the reactants and products in mass-weighted Cartesian coordinates. Subsequently, last structures from IRC were used to localize, optimize and characterize minima energy structures corresponding to reactant and product complexes.

2.5 Kinetic isotope effects (KIEs)

KIEs were computed for isotopic substitutions of key oxygen atoms, from the TSs and the reactant complexes localized with those SMs that showed a more realistic description of the reaction, as described into detail in the next section. Computational details can be found in previous publications [71].

3 Results

As described above, in this work we decided to analyse the possibilities and limitations of SMs in a controversial reaction involving a phosphate transfer from ATP cofactor to KanA. Three particular factors which could indicate the usefulness of SMs in this S_N2-like reaction were tested: (1) the shape of the PESs and barrier heights, $\Delta E^{\ddagger}_{(Pot)}$; (2) geometrical characteristics of the stationary structures, with particular attention to the TS structures; and (3) KIEs. Our analysis was based on the results of the different SMs employed to describe the QM subset of atoms in QM/MM calculations. In all cases, the reference results were those derived from the high level M06-2X/MM calculations.

First of all, as shown in Fig. 1, the M06-2X/MM PES obtained by controlling the two anti-symmetric combination of distances describing the proton transfer from KanA to Glu145 and the phosphorous transfer between the nucleophile atom (O4′) and leaving group (O3α) appears to render a proper description of the process. This PES, that is going to be considered as the reference one in the present study, shows two clear minimum energy regions that correspond to reactants complex (RC) and product complex (PC), according to their position on the surface and their values of the two axis. The optimized TS is localized on the quadratic region of the PES and connects the two stable states

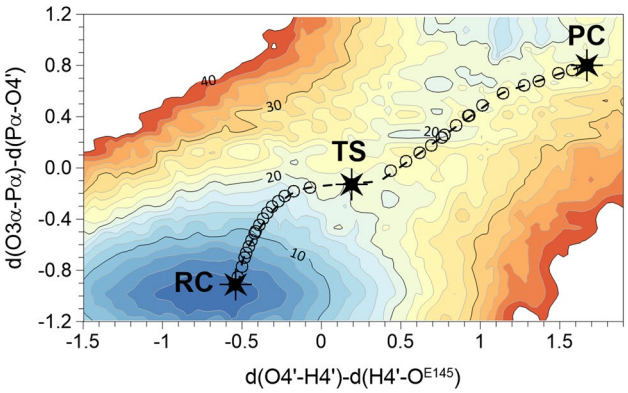

Fig. 1 M06-2X/MM PESs defined by the anti-symmetric combination of the distances describing the transfer of H4′ from O4′ to the oxygen of Glu145, and the anti-symmetric combination of the distances describing the nucleophilic attack of O4′ to Pα and the Pα-O3α bond cleavage. The black stars indicate the position of the M06-2X/MM localized and optimized RC, TS and PC, while the empty black circles indicate the position of the structures generated along the QM/MM IRC path

by an IRC path. The values of the reaction coordinates of the geometries generated along the QM/MM IRC path are displayed as circles in Fig. 1. Despite a deeper geometrical analysis of the different structures appearing as stationary point structures on the surface is carried out below, a preliminary analysis of the structures of the three states confirms that this high level method describes the reaction in a single step. The adenylyl group transfer from ATP-cofactor to the hydroxyl oxygen of KanA and the proton transfer from ANT4′ to Glu145 (see Scheme 1) takes place in a quite synchronous and concerted way (see the relative position of RC, TS and PC in Fig. 1). Once obtained the description of the reaction mechanism at high level of theory, next step in the present study was to evaluate the performance of the selected SMs methods. Figure 2 shows the resulting QM/MM PESs obtained when describing the QM subset of atoms with MNDO, AM1, PM3, RM1, MNDO/d, PM6, AM1/d-PhoT and DFTB3. As in Fig. 1, the localized TS structures are indicated in the PESs.

The **MNDO/MM PES** displayed in Fig. 2a shows a deficiency of the MNDO semiempirical Hamiltonian. Thus, analysis of the topology of the surface clearly shows how the process takes place in two steps, through a stable intermediate where the H4′ transfer from O4′ to the oxygen of Glu145 has been completed but the nucleophilic attack of the adenylyl group has not progressed (lower right corner of the PES). The corresponding TSs were optimized but both of them appear out of the surface: TS1 at coordinates −0.27 and −2.12 Å and TS2 at 2.22 and −0.55 Å (see Supporting Information for details).

The **AM1/MM PES** displayed in Fig. 2b apparently shows a concerted process. Nevertheless, analysis of the structures appearing on the putative PC region (right side of the surface) shows how the P-O3α is not completely broken. This particular *sp*-SM stabilize penta-coordinated phosphorous compounds and, consequently, the desirable product complex is not reached in a single step. The real PC would be located in the upper right white area of the surface, corresponding to a high-energy region at this level of theory.

The **PM3/MM PES** displayed in Fig. 2c renders similar description of the reaction as the AM1/MM method, where the stable structures optimized when the proton transfer is completed do not show the breaking of the P-O3α bond. Moreover, some additional artefacts are detected such as the limitation to properly localize a TS structure for the concerted nucleophilic attack and proton transfer, or the appearance of stable penta-coordinated phosphorous structures with the proton in between the donor O4′ and the acceptor O atom of Glu145 (see the unexpected valley in the centre of the surface).

The **RM1/MM PES** displayed in Fig. 2d suggests also the existence of stable penta-coordinated phosphorous structures. In addition, according to the position of the localized TS, this QM Hamiltonian provides an odd description of the reaction. Thus, the localized TS structure appears at a very early stage of the process, either from the point of view of the proton transfer (anti-symmetric combination ca. −0.5 Å) or the nucleophilic attack (anti-symmetric combination ca. −0.7 Å). Additionally, the same behaviour of over-stabilizing hypervalent intermediate structures was observed, as in the AM1/MM or PM3/MM PESs. This pentacovalent intermediate was previously observed for AM1 and PM3 methods in other studies [72, 73] and it was explained based on the presence of the artificially attractive core–core interactions. Additionally, in case of RM1 method, H4′ atom is not yet transferred in the pentacovalent intermediate (see Supporting Information for details).

The **PM6/MM PES** presented in Fig. 2e shows how the reparametrized PM6 method describe the reaction as a concerted process, similar to the high level M06-2X/MM PES displayed in Fig. 1. The PES, despite not being very smooth specially in the region of the product complex, allows for localization minimum energy region corresponding to the two completed transfers. In addition, a TS structure was optimized from a structure of the quadratic region with values of the two selected reaction coordinates that appear also in good agreement with the ones of the TS localized at M06-2X/MM. Nevertheless, it is important to point out how the values of the two reaction coordinates corresponding to RC and PC appear significantly closer to the TS than in the reference PES at DFT level.

The **MNDO/d/MM PES** presented in Fig. 2f shows how just the inclusion of *d* orbitals does not necessary to improve the description of the reaction. The topology of the PES describes the reaction taking place through a

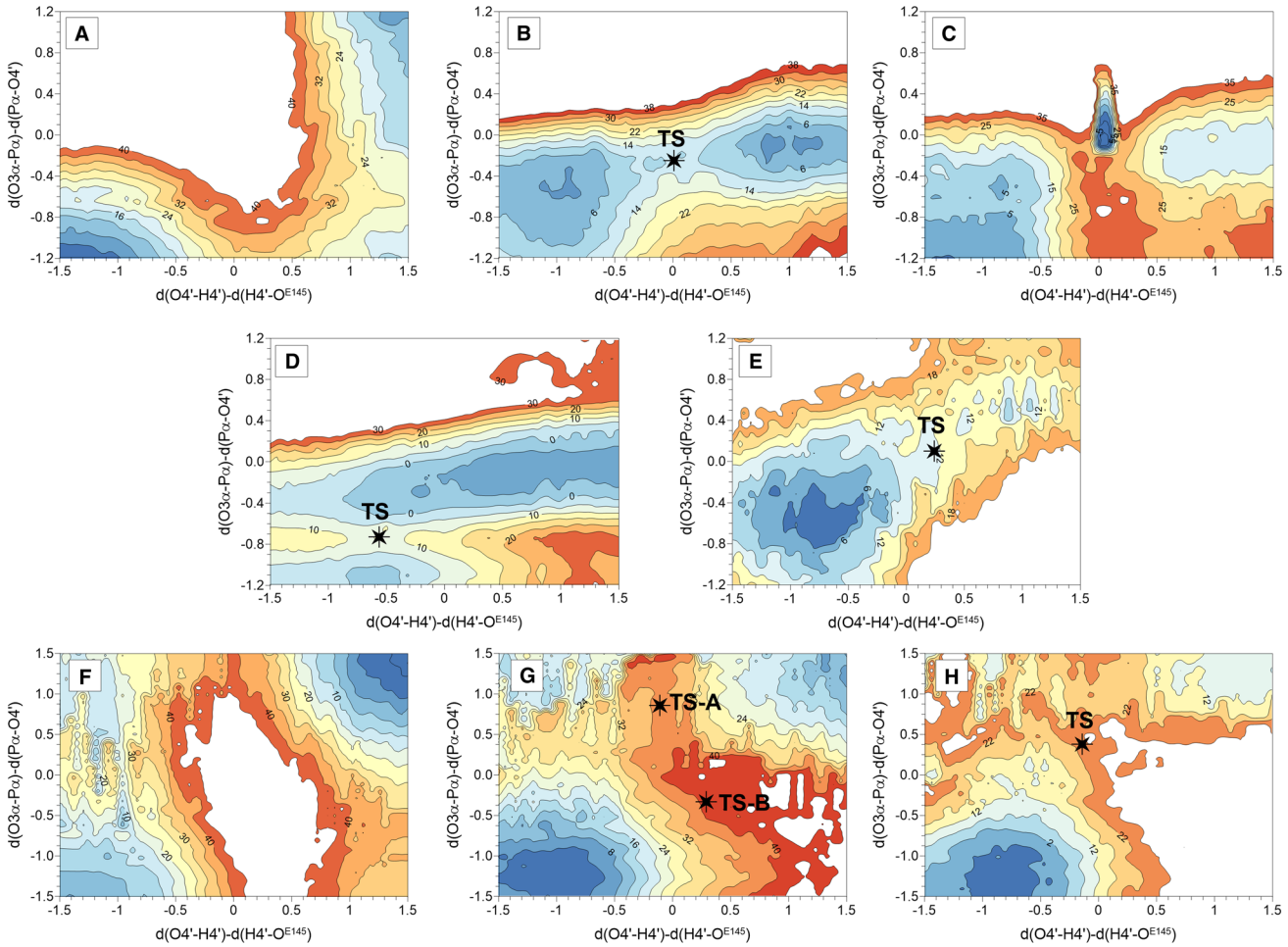

Fig. 2 QM/MM PESs for the Glu145-assisted mechanism of the adenylyl group transfer catalysed by ANT4′ obtained with the different SM to describe the QM subset of atoms: MNDO (**a**), AM1 (**b**), PM3 (**c**), RM1 (**d**), PM6 (**e**), MNDO/d (**f**), AM1/d-PhoT (**g**) and DFTB3 (**h**). The selected coordinates to obtain the PESs are the anti-symmetric combination of the distances describing the transfer of H4′ from O4′ to the oxygen of Glu145, and the anti-symmetric combination of the distances describing the nucleophilic attack of O4′ to Pα and the Pα-O3α bond cleavage. The positions of localized TS structures are indicated as black stars. Values of energy are given in kcal mol^{-1}. For clarity, areas of high energy of the PESs are shown in white

stable intermediate (upper left corner) where the adenylyl group is transferred without participation of Glu145. Thus, the reaction of adenylyl transfer occurs in a two-step manner; first the Pα-O3α is broken with simultaneous Pα-O4′ bond formation, followed by the abstraction of H4′ by the carboxyl oxygen of Glu145. This result provides completely different picture than the reaction mechanism derived from the DFT/MM studies. This is not a surprising result. Thus, despite the fact that MNDO/d method was shown to describe correctly transphosphorylation process under basic conditions [74, 75] where the acceptor is deprotonated and no hydrogen transfers are required, MNDO/d (as well as MNDO) is known to be problematic in the description of noncovalent intermolecular interactions because of the extensive repulsion just outside bonding distances [24].

This limitation of MNDO method was improved in *sp*-SMs (including AM1, PM3 and RM1). However, despite correction for hydrogen bonding with respect to MNDO method was done, neither AM1, PM3 nor RM1 improve the mechanistic description in case of the studied reaction. All three methods, although providing the concerted mechanism of a proton transfer from KanA to Glu145, and formation of the P-O4′, over-stabilize the pentacovalent intermediate preventing the P-O3α cleavage (see Supporting Information).

The **AM1d-PhoT/MM** PES, Fig. 2g, shows that the Glu145-assisted adenylyl transfer catalysed by ANT4′ reaction can take place as a concerted process. Nevertheless, the topology of the surface renders a minimum energy path much more asynchronous than the one obtained at M06-2X/MM level. The TS (TS-A in Fig. 2g) located in the quadratic region is characterized by a proton transfer in a very

advanced stage of the phosphorous transfer. In fact, structures where the phosphorous is completely transferred and the proton is not yet abstracted by Glu145 can be localized in the upper left corner of the surface.

Finally, the SM derived in the framework of DFT **DFTB3/MM** allows getting a PESs that also describes the phosphorous transfer and the proton transfer in a concerted manner, as shown in Fig. 2h. As in the case of the AM1/d-PhoT, DFTB3 describes a quite asynchronous mechanism, by comparison with the one obtained at M06-2X/MM level: the proton transfer occurs in an advanced stage of the phosphorous transfer in the TS (reaction coordinate for the phosphorous transfer equal to 0.5 Å).

In all, the preliminary analysis of the different tested SMs, based on the topology of the corresponding PESs, shows how PM6, AM1/d-PhoT and DFTB3 semiempirical Hamiltonians (Fig. 2e, g and h, respectively) provide a description of the mechanism in agreement with the topology of the PES obtained at M06-2X/MM level (Fig. 1).

Qualitatively equivalent behaviour of the different tested SMs were observed in case of the ATP-assisted reaction catalysed by ANT4′ (see Figure S1 of Supplementary Material), a less favourable mechanism according to previous high level QM/MM studies [52]. The PESs obtained at M06-2X/MM level and with the different tested SMs/MM methods are deposited in the supplementary material.

Key distances of the geometries of the stationary structures of the corresponding PESs optimized with the most promising SMs (PM6, AM1/d-PhoT and DFTB3), together with the reference values obtained at M06-2X/MM, are listed in Table 1. Coordinates of the TS structures are deposited in the supporting information. A More O'Ferrall-Jencks [76, 77] diagram based on the coordinates of RC, TS and PC is plotted in Fig. 3 for comparing these four methods.

According to the obtained optimized geometries, while PM6, AM1/d-PhoT and DFTB3 are capable of describing the reaction qualitatively equal to the description derived from M06-2X, significant differences can be highlighted. First of all, as mentioned above, PM6 tends to favour the optimization of RC and PC structures much closer to the TS than the rest of the methods. This behaviour reminds the one observed in the AM1, PM3 and RM1 methods that over-stabilized penta-coordinated structures of the phosphorous atom. Obviously, as discussed below, this effect will have a consequence in the energetics and KIEs. The second important conclusion is that, while the PM6 TS describes the S_N2 reaction as an associative concerted mechanism, same as the higher level M06-2X/MM method, AM1/d-PhoT and DFTB3 Hamiltonians renders dissociative concerted mechanisms (see Fig. 3). This result confirms some limitation of these methods to be used in computational studies of phosphate chemistry, as previously stated [27, 78]. Nevertheless, a unique behaviour is obtained with AM1/d- PhoT.

Table 1 Key distances (in Å) and angle (in degrees) in reactants complex, transition state, and products complex, localized at PM6/MM, AM1/d-PhoT/MM, DFTB3/MM and M06-2X/MM methods

	PM6	AM1/d-PhoT		DFTB3	M062X
Reactant complex					
d(Pα -O3α)	1.79	1.70		1.69	1.68
d(Pα –O4′)	2.24	3.16		2.92	2.59
d(O3α-O4′)	4.03	4.86		4.60	4.26
d(H4′-O^{E145})	1.68	2.84		1.87	1.55
d(H4′-O4′)	1.05	0.99		0.99	1.01
d(Pα-O1α)	1.51	1.53		1.50	1.50
d(Pα-O2α)	1.49	1.50		1.50	1.49
d(Pα-O5′)	1.66	1.63		1.65	1.60
MUE	0.1163	0.3213		0.1350	–
∢(O4′-Pα-O3α)	172.6	176.1		172.8	174.1
Transition structure					
		TS-A	TS-B		
d(Pα -O3α)	2.01	2.68	1.83	2.53	1.88
d(Pα –O4′)	1.91	1.82	2.16	2.15	2.01
d(O3α-O4′)	3.92	4.49	3.99	4.66	3.88
d(H4′-O^{E145})	1.17	1.35	1.14	1.29	1.14
d(H4′-O4′)	1.41	1.24	1.43	1.15	1.33
d(Pα-O1α)	1.52	1.51	1.53	1.47	1.51
d(Pα-O2α)	1.50	1.50	1.50	1.50	1.51
d(Pα-O5′)	1.66	1.64	1.64	1.61	1.62
MUE	0.0550	0.2413	0.0575	0.2450	–
∢(O4′-Pα-O3α)	174.6	173.1	174.7	169.4	174.7
Product complex					
d(Pα -O3α)	2.18	2.90		3.00	2.46
d(Pα –O4′)	1.79	1.66		1.66	1.66
d(O3α-O4′)	3.97	4.54		4.63	4.10
d(H4′-O^{E145})	1.07	1.01		0.99	0.99
d(H4′-O4′)	1.66	2.07		1.88	2.66
d(Pα-O1α)	1.52	1.53		1.52	1.52
d(Pα-O2α)	1.50	1.52		1.52	1.50
d(Pα-O5′)	1.67	1.65		1.64	1.61
MUE	0.2100	0.1950		0.2375	–
∢(O4′-Pα-O3α)	172.4	169.1		167.0	168.2

The mean unsigned errors (MUE) were calculated for the eight key distances at PM6/MM, AM1/d-PhoT/MM and DFTB3/MM level, relative to the benchmark M06-2X/MM calculations

Interestingly, a different TS structure was also optimized with this SM as a saddle point of order one when starting the optimization from the coordinates of the TS localized at M06-2X/MM. This structure, labelled as TS-B in Fig. 2g, is quite close to the starting reference TS structure optimized at M06-2X/MM. The IRC path traced down from this second TS-B connected RC and PC. It is important to mention that the same strategy was employed with PM6/MM and DFTB3/MM but the final optimized TS structures in these two cases were almost coincident with the ones obtained when starting

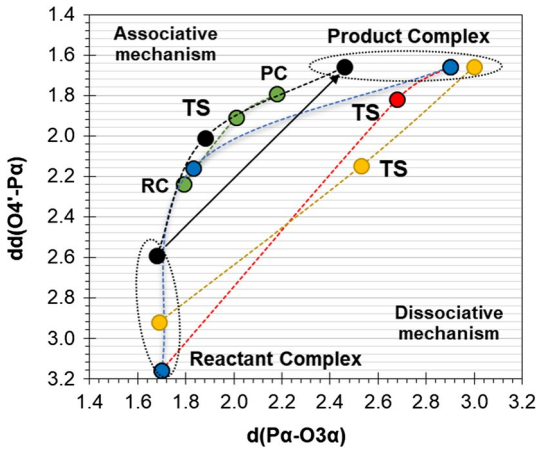

Fig. 3 More O'Ferrall-Jencks diagram generated from the results derived from PM6/MM (green), AM1/d-PhoT/MM (TS-A and TS-B in red and blue, respectively), DFTB3/MM (yellow) and M06-2X/MM (black) methods. Positions of localized RC, TS and PC are indicated as circles. Black arrow indicates the hypothetical perfectly synchronous concerted mechanism

from geometries selected from the quadratic regions of the corresponding PESs.

An overall deviation of the geometries obtained with each SM, by comparison to the M06-2X/MM method, can be summarized by computing the mean unsigned error (MUE) calculated for the eight key distances selected in Table 1. According to the results, AM1/d-PhoT would be the method that provides the TS closest to the M06-2X/MM level. Nevertheless, this is the case when starting from an already known optimized structure at this high level of theory (TS-B), which is usually not the case for most of the computational studies. When using the TS-A, which is the TS deduced from the PES, the deviations are similar to those obtained with DFTB3. PM6 provides reasonable low values of MUE at the TS. All methods provide similar MUE for the PC while for RC AM1/d-PhoT gives significantly higher deviations than PM6 and DFTB3.

An analysis of energetics can be done based on the structures optimized at each level of theory. A note of caution must be introduced at this point since, as well known, statistical simulations must be carried out for systems containing a huge number of degrees of freedom such as enzymes, to get values (free energies) directly compared with experiments. Comparison of energies of single molecules can render dramatic differences due to the high dimensionality of the problem [79, 80] as also confirmed by single molecule spectroscopy [81]. Anyway, an approximate estimation of the accuracy of the methods can be obtained from the comparison of the results derived from the PES. Thus, according to the values listed in Table 2, PM6 would be the best SM method, rendering the closest values of activation and reaction energies, with respect to the reference M06-2X method.

Table 2 Relative potential energy (ΔE) computed at PM6/MM AM1/d-PhoT/MM, DFTB3/MM and M06-2X/MM methods

	PM6	AM1/d-PhoT	DFTB3	M06-2X
RC	0.0	0.0	0.0	0.0
TS	15.1	57.3/89.7	45.6	9.8
PC	1.1	7.4	8.7	−0.7

The two values of the relative energy of the TS at AM1/d-PhoT level correspond to the two optimized structures TS-A and TS-B (see text for details). All values are in kcal mol^{-1}

Nevertheless, as mentioned above, this is due to the fact that PM6 optimize structures of either RC and PC that are significantly closer to the TS than the corresponding structures optimized with the rest of methods. RC and PC structures obtained at PM6/MM have a high penta-coordinated phosphorous character.

3.1 Kinetic isotope effects

Finally, KIEs were computed for the isotopic $^{16}O/^{18}O$ substitutions at the bridge and non-bridge oxygen atoms (see Scheme 1). We must keep in mind that KIEs, together with rate constants, are magnitudes that can be directly compared with experiments to support the theoretically proposed reaction mechanisms. The results are summarized in Table 3 and Fig. 4. As expected, the primary $^{16}O/^{18}O$ KIEs of the O-bridge atoms are much higher than the secondary $^{16}O/^{18}O$ KIEs of the O-non-bridge atoms. PM6/MM, related with the comments on the structures of RC and TS stressed above (RC is dramatically close to the optimized TS), renders KIEs significantly lower than the rest of the methods. These values deviate significantly from the reference values obtained at M06-2X/MM level [52], which were shown to be in very good agreement with experimental data [82]. Regarding the KIEs derived from the AM1/d-PhoT/MM and DFTB3/MM calculations, it is reliable how the former agrees pretty well

Table 3 Kinetic isotope effects (KIEs) computed at PM6/MM AM1/d-PhoT/MM, DFTB3/MM and M06-2X/MM methods methods at 300 K

	PM6	AM1/d-PhoT		DFTB3	M06-2X
^{18}O-bridge					
		TS-A	TS-B		
O4′	1.0038	0.9873	0.9992	1.0243	1.0204
O3α	1.0017	1.0141	1.0081	1.0056	1.0121[a]
^{18}O-non-bridge					
O5′	0.9998	1.0043	0.9987	0.9956	1.0026[a]
O1α	1.0001	0.9995	1.0002	0.9965	1.0000[a]
O2α	1.0001	1.0053	1.0031	0.9967	0.9981[a]

[a]values from Ref. [52]

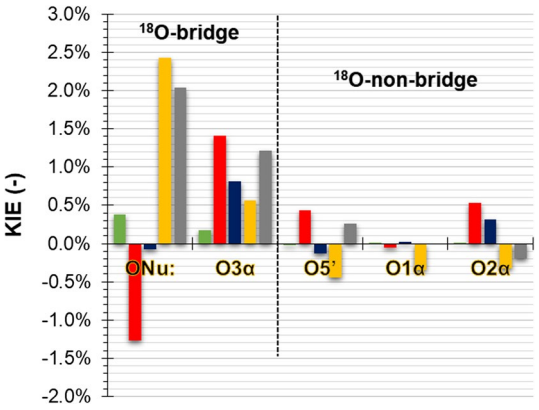

Fig. 4 Deviations from no kinetic isotope effect (KIEs), in %, computed for bridge and non-bridge isotopically substituted oxygen atoms at PM6/MM (green), AM1/d-PhoT/MM (from TS-A in red, from TS-B in blue), DFTB3/MM (yellow) and M06-2X/MM (grey) methods. Positive values (+) and negative values (−) correspond to normal and inverse KIEs, respectively

with the M06-2X/MM results for the substitution on O3α, especially when using the TS-B structure. When using the TS-A, the KIEs are obviously not so close and, in any case, an opposite behaviour (inverse KIEs) is obtained for the substitution on O4'. DFTB3 provides reasonable values of primary KIEs. Regarding the secondary KIEs computed at M06-2X/MM level, isotopic substitution on O1α gives no KIE, slightly normal KIE at O5' and inverse KIEs at O3α. None of the SMs provide this trend which is in agreement with previous observations indicating that, for instance, the minimal basis inherent to all SMs limits the accuracy of computed IR and Raman intensities [83, 84]. Nevertheless, taking into account the low values of the computed secondary KIEs, small deviations could be obtained if exploring an statistical number of structures for each method.

3.2 DNA 3′-end processing reaction

In view of the results obtained with the different SMs employed in QM/MM schemes for the S_N2-like reaction of an adenylyl group transfer catalysed by ANT4′, an additional test was carried out for a similar phosphate transfer reaction between oxygen atoms. In particular, the selected reaction was the hydrolysis of phosphodiester bond at the 3′-end of the viral DNA (*v*DNA), as shown in Scheme 3.

Previous studies on this reaction at M06-2X/MM level showed that, in contrast to adenylyl group transfer, this reaction takes place in a two-step manner with formation of penta-coordinated phosphorus intermediate [85]. Then, this reaction can be considered as an extension of the present systematic analysis of the SMs and it can serve as a good benchmark to test their performance in obtaining

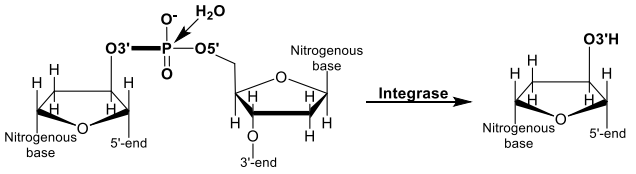

Scheme 3 Reaction of DNA 3′-end processing catalysed by PFV-IN

proper QM/MM PESs. The corresponding QM/MM PESs are shown in Figures S3-S5 of the Supplementary Material.

In the first step of *v*DNA 3′-end processing reaction where the oxygen of water molecule attacks phosphorus atom and one of its proton is transferred to the oxygen of phosphate group, AM1, PM3 and RM1 methods were found to provide very similar behaviour to those observed in the phosphorus transfer catalysed by ANT4′. Both of them provide structure of reactant complex in very advance stage (O^{Nu}-P bond much shorter) and, additionally, the penta-coordinated phosphorus structure of the intermediate was found to be over stabilized, by comparison with the results obtained with the DFT method. AM1/d-Pho-T and DFTB3 are providing very asynchronous picture of the reaction progress, both describing position of the TS corresponding to O^{Nu}-P bond formation with a very advance proton transfer to O3′ of scissile bond. Additionally, very shallow minima were found in the PES area corresponding to the intermediate structure. The most promising description of the first step was however obtained using PM6 SM. The computed profile derived from the PES at PM6/MM is in fact very similar to that obtained at DFT level. The description of the second step with the different methods is in agreement with the corresponding performance on the first step: those over stabilizing the penta-coordinated intermediate show a clear minimum energy area in the intermediate (AM1, PM3 and RM1), PM6, AM1/d-PhoT and DFTB3 provide a rough PES where the location of the stationary point structures is not clearly defined.

4 Conclusions

This work inspects the correctness of standard available semiempirical methods, such as MNDO, AM1, PM3, RM1, PM6, MNDO-d, AM1/d-PhoT, together with a semiempirical density functional theory based method, DFTB3. These QM methods have been employed in QM/MM studies of the E145-assisted adenylyl transfer catalysed by ANT4' enzyme. Their usefulness in the study of this type of reactions is assessed on the basis of reference results obtained at M06-2X/MM level of theory.

The analysis of the QM/MM PESs explored for all these methods shows the limitations of the *sp*-SMs to describe this

kind of reactions, which involve the transfer of a phosphor atom. This result would be in agreement with the conclusions obtained by Marcos et al. when revisiting penta-coordinated phosphorus compounds by high-level QM/MM calculations [28]. The MNDO as well as its improved MNDO/d version describes the process in two steps through a stable intermediate where the adenylyl group is transferred without participation of the base, Glu145, despite in different timing. This behaviour is inverse to the one provided by the PM3 method that stabilize structures where the proton transfer is completed before the breaking of the Pα-O3α bond takes place. In addition, some artefacts are detected in PM3 such as the limitation to properly localize a TS structure for the concerted nucleophilic attack and proton transfer, or the appearance of stable penta-coordinated phosphorous structures. AM1 provides a concerted process mechanism but the PC region corresponds to structures where Pα-O3α is not completely broken (i.e., penta-coordinated phosphorous structures as those located with PM3). RM1 suggests also the existence of stable penta-coordinated phosphorous structures, not describing a stable structure for the Pα-O3α bond breaking. The rest of tested SMs describes both transfers in a concerted way but with different limitations. Thus, PM6 stabilizes structures of RC and PC with values of the two reaction coordinates significantly closer to the TS than in the reference PES at DFT level. Finally, both AM1/d-PhoT and DFTB3 are capable of describing the full process catalysed by ANT4′ as a Glu145-assisted adenylyl transfer reaction in a concerted manner. Nevertheless, the topology of the PES of the former indicates that the minimum energy path appears to be much more asynchronous than the one obtained at M06-2X/MM level. A much more asynchronous process was already detected in previous studies of phosphate transfer when employing AM1/d-PhoT, by comparison with higher level of theory [4, 29, 30]. In the present study, structures where the phosphorous is completely transferred and the proton is not yet abstracted by Glu145 can also be localized with this method. This is not the case with DFTB3, where the proton transfer occurs in an advanced stage through a more dissociative phosphorous transfer TS. Interestingly, a unique behaviour is obtained with AM1/d-PhoT, which is capable of localizing different TS structures when starting the optimization from the coordinates of the TS localized at M06-2X/MM.

Apart from the exploration of the ATP-assisted reaction catalysed by ANT4′, an additional system, the 3′end DNA processing reaction catalysed by PFV Integrase, was selected to confirm the conclusions on the performance of the different selected SMs in a different phosphate transfer reaction. The behaviour of the tested SMs observed in the S_N2-like reaction of the adenylyl group transfer catalysed by ANT4′ were qualitatively reproduced in this two steps reaction.

Further analysis of the results obtained with the most promising SMs (PM6, AM1/d-PhoT and DFTB3) were based on the comparison of the energetics and KIEs. The potential energy barriers are all much higher than the one obtained at M06-2X level with the exception of PM6. Nevertheless, this can be considered as a fortuitous result derived from the character of the localized TS, with reaction coordinates dramatically close to the TS. The isotopic $^{16}O/^{18}O$ substitutions at the bridge and non-bridge oxygen atoms allow computing primary and secondary KIEs. The KIEs obtained at PM6 are all very small, obviously as a consequence of the located structures of RC, very close to the TS. DFTB3/MM calculations provide primary KIEs in good agreement with the M06-2XMM level, while the accuracy of AM1/d-PhoT depends on the particular TS structure selected to perform the KIEs calculations. In addition, an inverse primary KIE is obtained with this SM, basically due to the fact that the RC is significantly further from the phosphorous atom than the RC structures obtained with the M06-2X method. Regarding the secondary KIEs, none of the SMs provide the same trend of values as the one obtained at M06-2X. Nevertheless, taking into account the low values of the computed secondary KIEs, small deviations could be obtained if exploring a statistical number of structures for each method. Anyway, the shape of the free energy surfaces derived from these statistical simulations will be determined by the corresponding PESs and, consequently, the present study can be considered as a proper benchmark [4].

As a final conclusion, this test of SMs in QM/MM calculations reveals that SMs require further improvements since they are still failing in properly describing a crucial phosphorous involved enzyme catalysed reaction. An inadequate description of the intra and intermolecular interactions and the corresponding biased distribution of the electronic density in the groups involved in the chemical reaction must be at the origin of the problems. Nevertheless, the present study provides evidences of the value of some of the most recent SMs to be able to generate structures that can be used as starting points for methods at higher level of theory.

Acknowledgements This work was supported by the Spanish Ministerio de Ciencia, Innovación y Universidades (Grant PGC2018-094852-B-C21), Universitat Jaume I (Project UJI B2017- 31). KŚ thanks the MINECO for a Juan de la Cierva—Incorporación (Ref. IJCI-2016-27503) contract. Authors acknowledge computational resources from the Servei d'Informàtica of Universitat Jaume I.

References

1. Masgrau L, Truhlar DG (2015) Acc Chem Res 48:431–438
2. Świderek K, Tuñón I, Moliner V (2014) WIREs Comput Mol Sci 4:407–421
3. Świderek K, Ruiz-Pernía JJ, Moliner V, Tuñón I (2014) Curr Opin Chem Biol 21:11–18

4. Mlyńsky V, Banaś P, Šponer J, van der Kamp MW, Mulholland AJ, Otyepka M (2014) J Chem Theory Comput 10:1608–1622
5. Krzemińska A, Moliner V, Świderek K (2016) J Am Chem Soc 138:16283–16298
6. Higashi M, Truhlar DG (2009) J Chem Theory Comput 5:2925–2929
7. Singh UC, Kollman PA (1986) J Comput Chem 7:718–730
8. Warshel A, Levitt M (1976) J Mol Biol 103:227–249
9. Martí S, Andrés J, Moliner V, Silla E, Tuñón I, Bertrán J (2008) J Am Chem Soc 130:2894–2895
10. Martí S, Andrés J, Moliner V, Silla E, Tuñón I, Bertrán J (2009) J Am Chem Soc 131:16156–16161
11. Świderek K, Tuñón I, Williams IH, Moliner V (2018) J Am Chem Soc 140:4327–4334
12. Świderek K, Martí S, Moliner V (2014) ACS Catal 4:426–434
13. Świderek K, Tuñón I, Martí S, Moliner V (2015) ACS Catal 5:1172–1185
14. Doron D, Major DT, Kohen A, Thiel W, Wu X (2011) J Chem Theory Comput 7:3420–3437
15. Vardi-Kilshtain A, Major DT, Kohen A, Engel H, Doron D (2012) J Chem Theory Comput 8:4786–4796
16. Major DT, Nam K, Gao J (2006) J Am Chem Soc 128:8114–8115
17. Liu CT, Layfield JP, Stewart RJ III, French JB, Hanoian P, Asbury JB, Hammes-Schiffer S, Benkovic SJ (2014) J Am Chem Soc 136:10349–10360
18. Świderek K, Arafet K, Kohen A, Moliner V (2017) J Chem Theory Comput 13:1375–1388
19. Lopez-Canut V, Roca M, Bertran J, Moliner V, Tuñón I (2011) J Am Chem Soc 133:12050–12062
20. Christensen AS, Kubař T, Cui Q, Elstner M (2016) Chem Rev 116:5301–5337
21. Petrovic D, Szeler K, Kamerlin SCL (2018) Chem Commun 54:3077–3089
22. Bordes I, García-Junceda E, Sánchez-Moreno I, Castillo R, Moliner V (2017) Int J Quantum Chem 118:e25520
23. Lopez-Canut V, Roca M, Bertran J, Moliner V, Tuñón I (2010) J Am Chem Soc 132:6955–6963
24. Nam K, Cui Q, Gao J, York DM (2007) J Chem Theory Comput 3:486–504
25. Arantes GM, Loos M (2006) Phys Chem Chem Phys 8:347–353
26. Lopez X, York DM (2001) Theo Chem Acc 109:149–159
27. Yang Y, Yu H, York D, Elstner M, Cui Q (2008) J Chem Theory Comput 4:2067–2084
28. Marcos E, Anglada JM, Crehuet R (2008) Phys Chem Chem Phys 10:2442–2450
29. Marcos E, Field MJ, Crehuet R (2010) Proteins 78:2405–2411
30. Murillo-López J, Zinovjev K, Pereira H, Caniuguir A, Garratt R, Babul J, Recabarren R, Alzate-Morales J, Caballero J, Tuñón I, Cabrera R (2019) Chem Sci 10:2882–2892
31. Dewar MJS, Thiel W (1977) J Am Chem Soc 99:4899–4907
32. Dewar MJS, Zoebisch EG, Healy EF, Stewart JJP (1985) J Am Chem Soc 107:3902–3909
33. Stewart JJP (1989) J Comput Chem 10:209–221
34. Rocha GB, Oliveira Freire R, Simas AM, Stewart JJP (2006) J Comput Chem 27:1101–1111
35. Thiel W, Voityuk AA (1992) Theor Chim Acta 81:391–404
36. Thiel W, Voityuk AA (1996) J Phys Chem 100:616–626
37. Bernal-Uruchurtu MI, Martins-Costa MTC, Millot C, Ruiz-López MF (2000) J Comput Chem 21:572–581
38. Bernal-Uruchurtu MI, Ruiz-López MF (2000) Chem Phys Lett 330:118–124
39. Harb W, Bernal-Uruchurtu MI, Ruiz-López MF (2004) Theor Chem Acc 112:204–216
40. Arillo-Flores OI, Ruiz-López MF, Bernal-Uruchurtu MI (2007) Theor Chem Acc 118:425–435
41. Stewart JJP (2007) J Mol Model 13:1173–1213
42. Stewart JJP (2009) J Mol Model 15:765–805
43. Marion A, Monard G, Ruiz-López MF, Ingrosso F (2014) J Chem Phys 141:034106
44. Imhof P, Noé F, Fischer S, Smith JC (2006) J Chem Theory Comput 2:1050–1056
45. Wahiduzzaman M, Oliveira AF, Philipsen P, Zhechkov L, van Lenthe E, Witek H, Heine T (2013) J Chem Theory Comput 9:4006–4017
46. Gaus M, Lu X, Elstner M, Cui Q (2014) J Chem T Theory Comput 10:1518–1537
47. Gaus M, Goez A, Elstner M (2013) J Chem Theory Comput 9:338–354
48. Gaus M, Cui Q (2012) Elstner. J Chem Theory Comput 7:931–948
49. Editorial (2013) The antibiotic alarm. Nature 495:141
50. Berendonk TU, Manaia CM, Merlin C, Fatta-Kassinos D, Cytryn E, Walsh F et al (2015) Nat Rev Microbiol 13:310–317
51. Becker B, Matthew A (2013) ACS Chem Biol 8:105–115
52. Martí S, Bastida A, Świderek K (2019) Front Chem 6:660
53. Zhao Y, Truhlar DG (2008) Acc Chem Res 41:157–167
54. Zhao Y, Truhlar DG (2008) Theor Chem Acc 120:215–241
55. Bordes I, Ruiz-Pernía JJ, Castillo R, Moliner V (2015) Org Biomol Chem 13:10179–10190
56. Bordes I, Castillo R, Moliner V (2017) J Phys Chem B 121:8878–8892
57. Pedersen LC, Benning MM, Holden HM (1995) Biochemistry 34:13305–13311
58. Olsson MHM, Sondergaard CR, Rostkowski M, Jensen JH (2011) J Chem Theory Comput 7:525–537
59. Duan Y, Wu C, Chowdhury S, Lee MC, Xiong G, Zhang W, Kollman P et al (2003) J Comput Chem 24:1999–2012
60. Field MJ, Albe M, Bret C, Proust-De Martin F, Thomas A (2000) J Comput Chem 21:1088–1100
61. Krzemińska A, Paneth P, Moliner V, Świderek K (2015) J Phys Chem B 119:917–927
62. Jorgensen WL, Chandrasekhar J, Madura JD, Impey RW, Klein ML (1983) J Chem Phys 79:926–935
63. Stewart JJP (1996) Quantum Chem Progr Exch 455:6
64. Case DA, Betz RM, Cerutti DS, Cheatham TE III, Darden TA, Duke RE, Giese TJ, Gohlke H, Goetz AW, Homeyer N, Izadi S, Janowski P, Kaus J, Kovalenko A, Lee TS, LeGrand S, Li P, Lin C, Luchko T, Luo R, Madej B, Mermelstein D, Merz KM, Monard G, Nguyen H, Nguyen HT, Omelyan I, Onufriev A, Roe DR, Roitberg A, Sagui C, Simmerling CL, Botello-Smith WM, Swails J, Walker RC, Wang J, Wolf RM, Wu X, Xiao L, Kollman PA (2016) AMBER 2016. University of California, San Francisco
65. Byrd RH, Lu P, Nocedal J, Zhu C (1995) J Sci Comput 16:1190–1208
66. Baker J, Kessi A, Delley BJ (1996) Chem Phys 105:192–212
67. Baker J (1997) J Comput Chem 18:1079–1095
68. Martí S, Moliner V, Tuñón I, Williams IH (2005) J Phys Chem B 109:3707–3710
69. Martí S, Moliner V, Tuñón I (2005) J Chem Theory Comput 1:1008–1016
70. Fukui K (1981) Acc Chem Res 14:363–368
71. Świderek K, Martí S, Tuñón I, Moliner V, Bertran J (2015) J Am Chem Soc 137:12024–12034
72. Tubert-Brohman I, Guimaraes CRW, Jorgensen WL (2005) J Chem Theory Comput 1:817–823
73. Lopez X, York DM (2003) Theor Chem Acc 109:149–159
74. Gregersen BA, Lopez X, York DM (2003) J Am Chem Soc 125:7178–7179
75. Gregersen BA, Lopez X, York DM (2004) J Am Chem Soc 126:7504–7513
76. Jencks WP (1985) Chem Rev 85:511–527
77. O'Ferrall RM (1970) J Chem Soc B 274–277

78. Gaus M, Lu X, Elstner M, Cui Q (2014) J Chem Theor Comput 10:1518–1537
79. Turner JA, Moliner V, Williams IH (1999) Phys Chem Chem Phys 1:1323–1331
80. Ferrer S, Tuñón I, Martí S, Moliner V, García-Viloca M, González-Lafont A, Lluch JM (2006) J Am Chem Soc 128:16851–16863
81. Xue Q, Yeung ES (1995) Nature 373:681–683
82. Gerratana B, Cleland WW, Reinhardt LA (2001) Biochemistry 40:2964–2971
83. Kaminski S, Gaus M, Elstner M (2012) J Phys Chem A 116:11927–11937
84. Kaminski S, Giese TJ, Gaus M, York DM, Elstner M (2012) J Phys Chem A 116:9131–9141
85. Krzemińska A, Świderek K (2019) J Chem Inf Model 59:2995–3005